Z. Phys. B 101, 211–217 (1996)

ZEITSCHRIFT
FÜR PHYSIK B

Optical constants of gold and silver clusters in the spectral range between 1.5 eV and 4.5 eV

M. Quinten

1. Physikalisches Institut, RWTH Aachen, D-52056 Aachen, Germany

Received: 1 September 1995/Revised version: 5 February 1996

Abstract. Optical constants of gold and silver clusters of various sizes are determined from measurements of their optical extinction in the range from 1.5 eV to 4.5 eV photon energy. For this purpose, it is shown that the optical extinction by spherical clusters satisfies a Kramers–Kronig relation, yielding the second quantity needed for the determination of the complex dielectric constant ε of the cluster material. The dielectric constant is then obtained applying a generalized Newton-Raphson iteration method on the measured extinction data and the Kramers-Kronig data. The results show a clear dependence on cluster size, and also deviations from bulk dielectric constants in the range of the interband transitions. From the various ε-data, a "bulk" dielectric constant of gold and silver is obtained, which fits the positions of the cluster plasmons more precisely than bulk dielectric constants from the literature.

PACS: 36.40. + d; 78.20.Ci; 82.70.Dd

1. Introduction

Small particles and inorganic clusters have been a major subject of interest in many investigations over the last three decades. Some exciting results and hypotheses on various properties of clusters have been formulated during this time. Looking in particular at optical properties, the most exciting phenomenon is the surface plasmon in clusters of silver, gold, copper, aluminum and alkali metals, which is easily established from optical extinction measurements. However, interpretations of measured spectra with concepts of classical electrodynamics, i.e. the Mie-theory for spheres [1] or the Rayleigh–Gans theory for ellipsoidal clusters [2], often fail, because these models require the optical constants of the cluster material. For clusters, the optical constants are modified with respect to bulk matter due to size and quantum size effects [3–11].

The determination of the optical constants of clusters with methods that work well for bulk, e.g. ellipsometry or electron energy loss spectroscopy, is rendered more difficult, as it is hardly possible to measure on single isolated clusters. A promising method for the determination of optical constants seems to be the measurement of optical extinction by the clusters, and the evaluation of the dielectric constant from these data using a Kramers–Kronig analysis.

In this paper, a method is described which is based on a Kramers–Kronig relation for the extinction, yielding a new quantity, which is needed for the evaluation of the dielectric constant. The dielectric constant is then obtained by applying a generalized Newton–Raphson iteration method on the measured extinction and the Kramers–Kronig data. With this method, the dielectric constant of several gold and silver clusters is obtained in the spectral range from 1.5 eV and 4.5 eV. The data extend the results of Kreibig [12, 13] to larger clusters and to a much wider spectral range, including also the region of interband transitions. From the obtained data, "bulk" dielectric constants are derived which allow a generally improved interpretation of the optical extinction and scattering spectra of gold and silver clusters.

Section 2 gives a brief introduction to the optical extinction by ensembles of spherical clusters. In Sect. 3, a Kramers–Kronig relation is derived for the extinction. It yields a new quantity P which is needed for the evaluation of the dielectric constant ε. In Sect. 4, the method for the evaluation of ε is presented. Results for the dielectric constant of several gold and silver clusters are exposed and discussed in Sect. 5. In Sect. 6, a conclusion is given.

2. Optical extinction by ensembles of clusters

Optical extinction of light with photon energy $\hbar\omega$ by an isolated spherical particle of diameter 2a is described by the extinction cross-section

$$C_{\text{ext}}(\omega, a) = \frac{2\pi c^2}{\omega^2 \varepsilon_{\text{M}}(\omega)} \sum_{n=1}^{\infty} (2n+1)\ \text{Re}(a_n + b_n), \tag{1}$$

following the concepts of classical electrodynamics (Mie-theory [1]). In this equation, c is the vacuum velocity of

light, $\varepsilon_M(\omega)$ accounts for the dielectric constant of the host medium and Re means the real part. The scattering coefficients a_n of the TM-mode of multipole order n, and b_n of the corresponding TE-mode, depend on the parameters $x = \omega/c\, a\sqrt{\varepsilon_M(\omega)}$ and $y = \omega/c\, a\sqrt{\varepsilon(\omega)}$, where the generally complex dielectric constant $\varepsilon(\omega) = \varepsilon_1(\omega) + i\varepsilon_2(\omega)$ of the particle enters the calculation.

For an ensemble of non interacting small particles, e.g. in a colloidal suspension, the extinction is

$$E(\omega) = -\log\left(\frac{I_t(\omega)}{I_0(\omega)}\right). \tag{2}$$

It is connected to the cross-section of (1) by Lambert–Beer's law,

$$E(\omega) = \sum_j C_{\text{ext}}(\omega, a_j)\,\frac{N_j}{V}\,d\cdot\log(e) \tag{3}$$

It is assumed that the ensemble consists of particles of different sizes $2a_j$ and concentrations N_j/V; d is the thickness and V is the total volume of the sample.

As the extinction depends on the dielectric constant $\varepsilon(\omega)$ of the particle material, it is not possible to directly determine $\varepsilon(\omega)$ from the inversion of the measured extinction data. For this purpose, a Kramers Kronig relation must be derived which yields the second quantity $P(\omega)$, necessary for the separate evaluation of the real and imaginary part of $\varepsilon(\omega)$.

3. Kramers Kronig relation for the extinction by spherical clusters

According to a method given by Landau and Lifshitz [14] a Kramers-Kronig relation is derived for $E(\omega)$ and $P(\omega)$. Rather than the extinction $E(\omega)$, it is the sum over the scattering coefficients a_n and b_n in (1) that satisfy the conditions for a Kramers–Kronig relation.

Consider the complex function

$$F(\omega) = \frac{1}{\omega^2}\sum_{n=1}^{\infty}(2n+1)\,(a_n + b_n), \tag{4}$$

in the plane of complex frequencies $\Omega = \omega + i\delta$. Let ω_0 be a real and positive value. Then, the function

$$G(\omega) = \frac{F(\omega) - F(\infty)}{\omega - \omega_0} \tag{5}$$

can be integrated around a closed contour C, as illustrated in Fig. 1. The principal value of the integral along the real axis is given by

$$\wp\int_{-\infty}^{\infty} G(\omega)\,d\omega = i\pi[F(\omega_0) - F(\infty)], \tag{6}$$

presuming that $F(\omega)$ is analytic in the upper half plane. Decomposition of (6) into real and imaginary parts yields the connection between the real and imaginary parts of $F(\omega)$. Multiplication of (4) with $2\pi c^2/\varepsilon_M(\omega)$ and using (2) yields

$$P(\omega_0) = -\frac{1}{\pi}\wp\int_{-\infty}^{\infty}\frac{E(\omega)}{\omega - \omega_0}\,d\omega + P(\infty)$$

$$= \frac{2\pi c^2}{\omega_0^2\varepsilon_M(\omega_0)}\sum_{n=1}^{\infty}(2n+1)\,\text{Im}(a_n(\omega_0) + b_n(\omega_0)), \tag{7}$$

where Im means the imaginary part. Recall that ω takes only real, positive values. Then, $P(\omega_0)$ simply becomes

$$P(\omega_0) = -\frac{2\omega_0}{\pi}\wp\int_0^{\infty}\frac{E(\omega)}{\omega^2 - \omega_0^2}\,d\omega + P(\infty), \tag{8}$$

since $E(-\omega) = E(\omega)$. However, to use this relation, the regularity of F(ω) for $\omega \to 0$ and $\omega \to \infty$ must be checked.

Consider first the case $\omega \to \infty$. The parameters x and y entering the computation of a_n and b_n are then identical because

$$\lim_{\omega\to\infty}\varepsilon(\omega) = \lim_{\omega\to\infty}\varepsilon_M(\omega) = 1. \tag{9}$$

So, the coefficients a_n and b_n themselves vanish and $\lim_{\omega\to\infty}F(\omega) = 0$. In consequence, $P(\infty) = 0$.

For $\omega \to 0$, the coefficients a_n and b_n become

$$a_n \propto \omega^{2n+1}\,\frac{\varepsilon(\omega) - \varepsilon_M(\omega)}{\varepsilon(\omega) + \dfrac{n+1}{1}\,\varepsilon_M(\omega)}, \tag{10}$$

$$b_n \propto \omega^{2n+3}\,\frac{\varepsilon(\omega) - \varepsilon_M(\omega)}{\varepsilon(\omega) + \dfrac{n+2}{n+1}\,\varepsilon_M(\omega)}, \tag{11}$$

Both decrease with decreasing ω faster than the increase in the prefactor ω^{-2} of $F(\omega)$. Hence $\lim_{\omega\to 0} F(\omega) = 0$.

In applying (8) to measurements on systems containing isolated metallic clusters in suspension, one must take into account that:

- The spectral region in which the measured data are available is limited; consequently the Kramers–Kronig (KK-) integral must be divided into parts.
- Outside the measured spectral range, the KK-integral can only be approximated by computations according to the Mie-theory [1], using bulk optical constants.
- The missing optical constants at high and low photon energies hinder this computation. The corresponding integrals must be approximated.

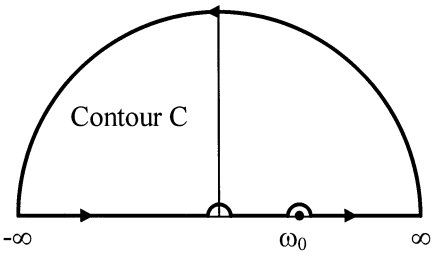

Fig. 1. Integration path along a closed contour C in the upper complex half plane

For these reasons, the complete integral is divided into five parts

$$P(\omega_0) = P_1(\omega_0) + P_2(\omega_0) \; + P_3(\omega_0) + P_4(\omega_0) + P_5(\omega_0)$$
$$= -\frac{2}{\pi}\left\{\int_0^{\omega_{\mathrm{FIR}}} \frac{E(\omega)d\omega}{\omega^2-\omega_0^2} + \int_{\omega_{\mathrm{FIR}}}^{\omega_{\mathrm{FIR}}} \frac{E(\omega)d\omega}{\omega^2-\omega_0^2} + \wp\int_{\omega_{\mathrm{IR}}}^{\omega_{\mathrm{UV}}} \frac{E(\omega)d\omega}{\omega^2-\omega_0^2}\right.$$
$$\left. + \int_{\omega_{\mathrm{UV}}}^{\omega_{\mathrm{FUV}}} \frac{E(\omega)\; d\omega}{\omega^2-\omega_0^2} + \int_{\omega_{\mathrm{FUV}}}^{\infty} \frac{E(\omega)\; d\omega}{\omega^2-\omega_0^2}\right\}, \qquad (12)$$

where $P_3(\omega_0)$ is the actual principal integral. $P_2(\omega_0)$ and $P_4(\omega_0)$ are obtained by computation using Mie's theory, with optical constants taken e.g. from Johnson and Christy [15] Hagemann et al. [16], or Olson and Lynch [17]. For continuity at $\omega = \omega_{\mathrm{IR}}$ and $\omega = \omega_{\mathrm{UV}}$, the computed spectra are multiplied with a factor that mainly takes into account the particle concentration in the colloidal suspension. $P_1(\omega_0)$ and $P_5(\omega_0)$ are estimated in the following way. Assuming that $\omega_{\mathrm{FIR}} \ll \omega_0$, or that $\omega_{\mathrm{FUV}} \gg \omega_0$,

$$P_1(\omega_0) \approx -\frac{2\omega_0}{\pi}\int_0^{\omega_{\mathrm{FIR}}} \frac{E(\omega)}{\omega_0^2} d\omega, \qquad (13)$$

$$P_5(\omega_0) \approx -\frac{2\omega_0}{\pi}\int_{\omega_{\mathrm{FUV}}}^{\infty} \frac{E(\omega)}{\omega_0^2} d\omega. \qquad (14)$$

As $E(\omega)$ decreases monotonically with decreasing ω as well as with the increasing ω, the integrand $E(\omega)$ is approximated either by $E(\omega_{\mathrm{FIR}})$, or by $E(\omega_{\mathrm{FUV}})$. It follows that

$$P_1(\omega_0) \approx -\frac{2}{\pi}\frac{\omega_{\mathrm{FIR}}}{\omega_0} E(\omega_{\mathrm{FIR}}), \qquad (15)$$

$$P_5(\omega_0) \approx \frac{2}{\pi}\frac{\omega_0}{\omega_{\mathrm{FUV}}} E(\omega_{\mathrm{FUV}}). \qquad (16)$$

It is clear that besides numerical inaccuracy, the computed values of $P(\omega)$ contain errors, because of the approximations in P_1, P_2, P_4 and P_5. Hence, to check the accuracy of this method, we first compute $E(\omega)$ and $P(\omega)$ for gold particles of diameter 2a = 20 nm using Mie's theory [1] in the energy range $\hbar\omega_{\mathrm{FIR}} = 0.855\,\mathrm{eV} \le \hbar\omega \le \hbar\omega_{\mathrm{FUV}} = 27.55\,\mathrm{eV}$, using optical constants from Johnson and Christy [15] and Olson and Lynch [17]. The values of $P_{\mathrm{KK}}(\omega)$ are then computed in the range $\hbar\omega_{\mathrm{IR}} = 1.5\,\mathrm{eV} \le \hbar\omega \le \hbar\omega_{\mathrm{UV}} = 4\,\mathrm{eV}$, using $E(\omega)$ from the above computations. This spectral range corresponds to that where extinction data from measurements are available. The results are then compared to the computed $P(\omega)$. In Fig. 2a, the values of $P(\omega)$ and $P_{\mathrm{KK}}(\omega)$ are compared, while Fig. 2b shows the contributions of the five integrals $P_1(\omega), \ldots, P_5(\omega)$. The main contribution comes from $P_3(\omega)$ as expected. However, also $P_4(\omega)$ contributes to a remarkable extent, in particular at larger photon energies. The contributions of $P_1(\omega)$ (far infrared) and $P_2(\omega)$ (infrared) are negligible and are unresolved in this plot. The differences between $P_{\mathrm{KK}}(\omega)$ and $P(\omega)$ are maximum at $\hbar_\omega = 2.32$ eV and 4 eV, where the relative error $(P_{\mathrm{KK}} - P)/P$ amounts to 3.6% and 7.9%, respectively. In the following it is assumed that the relative error in $P_{\mathrm{KK}}(\omega)$ is always smaller than 8%.

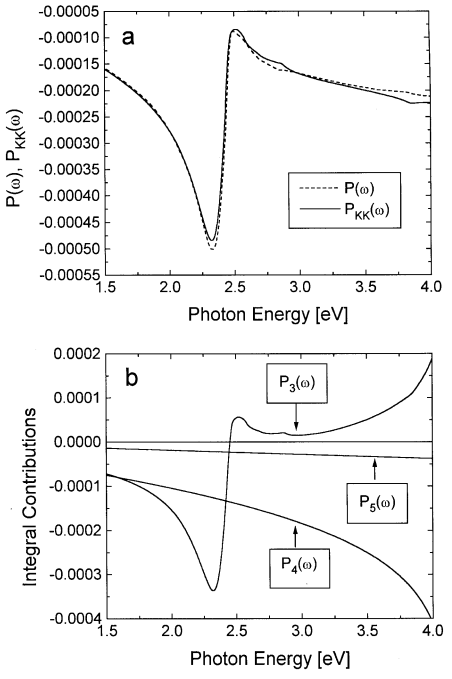

Fig. 2. **a** Computed spectra of $P(\omega)$ and $P_{\mathrm{KK}}(\omega)$ in the spectral range between 1.5 eV and 4 eV photon energy. **b** Partial integrals $P_1(\omega), \ldots, P_5(\omega)$ of the Kramers-Kronig integral

4. Evaluation of the dielectric constant with a generalized Newton-Raphson iteration method

After determination of $P(\omega)$ from $E(\omega)$, the complex dielectric constant $\varepsilon(\omega) = \varepsilon_1(\omega) + i\varepsilon_2(\omega)$ can be determined. For this purpose, an iterative method is used, the generalized Newton-Raphson iteration method (NRM). This is an effective method for finding zeros of transcendental functions. In its generalized form it is applicable to multidimensional systems of transcendental functions. For functions of complex arguments this method can simply be formulated, separating the real and imaginary parts. This provides a set of two equations for the $(j+1)$-th approximation to the zero, given the j-th approximation, the complex function $f = f_1 + if_2$, and the derivatives $\partial f_j/\partial y_k$:

$$\begin{pmatrix} y_1^{(j+1)} \\ y_2^{(j+1)} \end{pmatrix} = \begin{pmatrix} y_1^{(j)} \\ y_2^{(j)} \end{pmatrix} - \begin{pmatrix} h_{11} & h_{12} \\ h_{21} & h_{22} \end{pmatrix} \cdot \begin{pmatrix} f_1^{(j)} & (y_1^{(j)}, & y_2^{(j)}) \\ f_2^{(j)} & (y_1^{(j)}, & y_2^{(j)}) \end{pmatrix}. \qquad (17)$$

h_{ij} are the elements of the inverse Jacobi matrix. For complex numbers, the elements are connected to the derivative df/dy in a simple way, namely

$$h_{11} = h_{22} = \mathrm{Re}\left(\frac{df}{dy}\right) \Big/ \left|\frac{df}{dy}\right|^2, \qquad (18)$$

$$h_{12} = -h_{21} = \mathrm{Im}\left(\frac{df}{dy}\right) \Big/ \left|\frac{df}{dy}\right|^2, \qquad (19)$$

In our case, the function f is

$$\begin{pmatrix} f_1 \\ f_2 \end{pmatrix} = \begin{pmatrix} E_{\text{computed}}(y_1, y_2) - E_{\text{measured}} \\ P_{\text{computed}}(y_1, y_2) - P_{\text{KK}} \end{pmatrix} \tag{20}$$

It approaches zero if either $|f| \leq$ tolf or $|(y^{(j+i)} - y^{(j)})/y^{(j)}| \leq$ toly, where tolf and toly are the tolerances in finding a zero within the iteration. In the present analysis they were chosen as tolf ≤ 0.001, toly ≤ 0.005. Then, unavoidable measurement errors in the extinction ($\Delta E = 0.001$) and the error in the determination of $P_{\text{KK}}(\omega)$ (smaller than 8%) did not undermine the used NRM. On the other hand, the errors in ε_1 and ε_2 then became $\Delta\varepsilon_1 \leq 0.2$ and $\Delta\varepsilon_2 \leq 0.05$.

Finally, the complex dielectric constant is obtained from the zero $y^{(j+1)}$ from the relation

$$y^{(j+1)} = \frac{\omega}{c} a \sqrt{\varepsilon_1 + i\varepsilon_2}\,. \tag{21}$$

As initial guess for $y^{(0)}$, the dielectric constants from Johnson and Christy [15] were used in (21) :

$$y^{(0)} = \frac{\omega}{c} a \sqrt{\varepsilon_{1,\text{JC}} + i\varepsilon_{2,\text{JC}}}\,. \tag{22}$$

and $E_{\text{computed}}(y^{(0)})$ and $P_{\text{computed}}(y^{(0)})$ were computed using Mie's theory [1]. The next approach $y^{(1)}$ was obtained from these values and E_{measured} and P_{KK} using (17) and (20). Repeating for maximum 20 iterations, we arrived in the zero $y^{(j+1)}$, which yielded the dielectric constant from resolving (21).

5. Results and discussion

After having introduced the principles of the new method, we now present results obtained for small silver and gold clusters of various sizes. The particles are prepared in aqueous suspension by chemical reduction of silver from $AgNO_3$ following the recipe of Garbowski [18], and by chemical reduction of gold from chlorogold acid $HAuCl_4$ following the recipe of Zsigmondy [19]. Larger silver and gold particles are prepared in a second step using the smaller particles as nuclei for further precipitation of silver or gold. This method is described for gold by Zsigmondy [19] and is successfully adopted on silver. Transmission electron microscopy is applied to determine shape and size of the particles. In all examined samples the particles are approximately spherical. Their mean sizes are given in Table 1. The samples are numbered consecutively with respect to increasing size. In addition, a parameter A is given that accounts for the mean free path effect [3–11]. Its determination is described below. Extinction of light by the aqueous colloidal suspensions is measured using a common spectrophotometer. The measured extinction data are finally used in a Kramers–Kronig analysis as described in the previous section to determine the optical constants of the particles in the samples. In Fig. 3 the results for ε_1 and ε_2 of the various gold and silver particles are presented. For comparison, the data from Johnson and Christy [15] are also given as dashed line.

Table 1. Mean diameters 2a and mean free path parameters A for several gold and silver clusters

Sample	Mean diameter 2a [nm]	Mean free path parameter A
Au1	6.9	0.6
Au2	12.6	0.7
Au3	16	0.6
Au4	30.6	1.3
Au5	38	2
Ag1	16.6	2.5
Ag2	17.8	2.3
Ag3	20.4	2.5
Ag4	27.8	2
Ag5	32	3

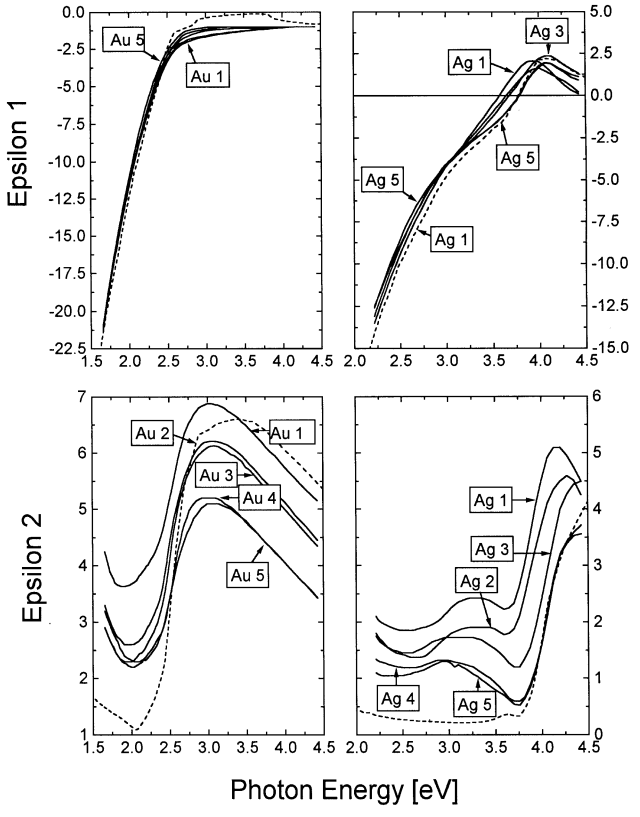

Fig. 3. Dielectric constants of various gold and silver clusters, obtained by Kramers-Kronig analysis of measured extinction data. For comparison, the dielectric constants of the data from Johnson and Christy [15] are plotted as dashed line

Apparently, the main deviation with respect to the bulk values occurs for the imaginary part ε_2. A clear dependence on particle size is recognized. With increasing particle size, ε_2 decreases, but does not approach the bulk value. These results agree with previous work of Kreibig [12, 13], who also derived quite similarly the dielectric constant of gold and silver clusters by a Kramers Kronig analysis. However, in the present paper the photon energy range where the optical constants are determined is strongly extended, including also the interband

transitions. Further, the particle size range is extended to much larger particles.

For interpretation of the data, we assume that the dielectric constant of the clusters is size-dependent and can be divided into a dielectric constant of the free electrons (Drude model) and a susceptibility which accounts for the interband transitions:

$$\varepsilon_{\text{cluster}}(\omega, a) = \varepsilon_{\text{Drude}}(\omega, a) + \chi_{\text{interband}}(\omega, a). \tag{23}$$

It can be assumed that the interband transitions begin to contribute to the dielectric constant at photon energies $\hbar\omega \geq \hbar\omega_{\text{IB}}$. At lower energies, the dielectric constant is

$$\varepsilon_{\text{cluster},1}(\omega, a) = \varepsilon_{\text{Drude},1}(\omega, a) + \chi_{\text{interband},1}(0)$$

$$= 1 + \chi_{\text{interband},1}(0) - \frac{\omega_p^2}{\omega^2 + \Gamma(a)^2}, \tag{24}$$

$$\varepsilon_{\text{cluster},2}(\omega, a) = \varepsilon_{\text{Drude},2}(\omega, a) = \frac{\Gamma(a)}{\omega}\frac{\omega_p^2}{\omega^2 + \Gamma(a)^2}. \tag{25}$$

ω_p is the bulk plasma frequency and $\Gamma(a)$ is the size-dependent damping constant, given according to the model of the mean free path effect [8, 9] as

$$\Gamma(a) = \Gamma_{\text{bulk}} + A\frac{v_F}{a}. \tag{26}$$

Γ_{bulk} is the bulk damping constant and v_F is the Fermi velocity in the metal. A is the mean free path parameter, which must be chosen appropriately. For photon energies $\hbar\omega \leq \hbar\omega_{\text{IB}}$, the parameter A as well as $\chi_{\text{interband},1}(0)$ can be determined for our samples from comparison of the dielectric constants of Fig. 3 with dielectric constants computed according to (24) and (25). In doing so, we find the parameters A given in Table 1.

The approach for the damping rate Γ in (26) is purely phenomenological, assuming that the electrons are additionally scattered at the surface after a time $\tau \sim a/v_F$. Almost all calculations which tried to explain this dependence [3–11] reproduced this damping rate, but with different parameters A. They are partly reviewed by Kreibig and Genzel [20].

The physical reason of this size-dependent damping are deviations from the model of a local dielectric constant near the surface. Improvements of the calculations of Kawabata and Kubo [5] were made for instance by Zaremba and Persson [21]. In their paper, the influence of a surface on the polarizability of a small metal particle in vacuum was considered in the random phase approximation. In summary, the surface induces an additional contribution to the Drude dielectric constant of the particle, separately from the bulk dielectric constant, making it nonlocal. Using the jellium model for the metal and introducing a surface polarization potential, which is missing in the work of Kawabata and Kubo [5], the authors found a damping rate proportional to 1/a. Assuming a step potential for concrete calculations, the surface induced relaxation time is obtained as $\tau = a/(3v_F)$, corresponding to $A = 3$! This value exceeds those obtained in the previous papers [3–11], where in most cases A is close to unity for spherical particles. Nevertheless, Kreibig [22] found that A can be larger than unity if the mean free path of the electrons is limited owing to grain-boundary scattering.

As it turns out from the work of Apell et al. [10] and Monreal et al. [11], the additional damping and thus A are material dependent, because it depends on the electron density in the particle. Hence, the damping should be influenced by physisorption, chemisorption or even chemical reactions at the particle surface, which induce changes of the density profile normal to the surface. There is strong evidence for such an influence from experiments by Charlé et al. [23], Kreibig [24], and most recently Hövel et al. [25], Hövel [26] and Hilger [27] for particles in matrices and Nusch [28] for particles with adsorbed molecules. In our case, it can be assumed that ions from the electrolyte and water molecules are physisorbed at the surface of the particles, leading to large halfwidths of the cluster plasmons.

In a recently published paper Persson [29] discussed the origin of this effect and extended the work of Zaremba and Persson [21] to include the influence of a layer of atoms or molecules associated with the matrix environment of the particle. Besides the surface induced damping already obtained by Zaremba and Persson [21], he found a contribution to the surface plasmon halfwidth which depends on the number of adsorbates per unit surface area and the frequency-dependent cross section σ_{diff} for diffusive scattering of the electrons by the adsorbates. The dominant contribution to σ_{diff} occurs if the adsorbate has a resonance state or virtual level at a distance $\sim\hbar\omega$ from the Fermi level, due to adsorbate-substrate coupling. With this assumption, Persson arrived in a good quantitative interpretation of the experimental data from Charlé et al. [23] and Kreibig [24]. In the present case of small gold and silver particles in aqueous suspension, these effects must also be considered, leading to large parameters A. However, from the preparation method, we do not know which and how many ions or water molecules are adsorbed at the surface of the particles, making it difficult to predict the amplitude of the parameter A. Particularly for silver, it seems that the adsorption of ions on the surface leads to an increased damping of the surface plasmon, resulting in parameters A between 2 and 3 in Table 1.

Although we found dielectric constants for several silver and gold clusters of various size, it is of more practical interest to have only one unique set of optical constants for all gold or silver clusters, which can be easily changed according to the model of the mean free path effect. To find such a unique set of opti&cal constants, the susceptibilities $\chi_{\text{interband}}$ were computed for each sample. For this purpose, the size-dependent Drude dielectric constant was subtracted from the dielectric constants of the clusters, using the mean free path parameters A from Table 1. The resulting curves for each $\chi_{\text{interband},1}$ and $\chi_{\text{interband},2}$ were quite close to each other, so that it was possible to obtain one representative mean curve $\chi_{\text{interband},1}$ and $\chi_{\text{interband},2}$ for each particle material. Addition of a bulk Drude dielectric constant, i.e. $\varepsilon_{\text{Drude}}(\omega, \infty)$, finally yielded „bulk“ dielectric constants of gold and silver clusters. The obtained values are plotted in Fig. 4 in comparison to the data from Johnson and Christy [15]. Again, it is to recognize, that the real part ε_1 coincides quite good with the real part of the data from Johnson

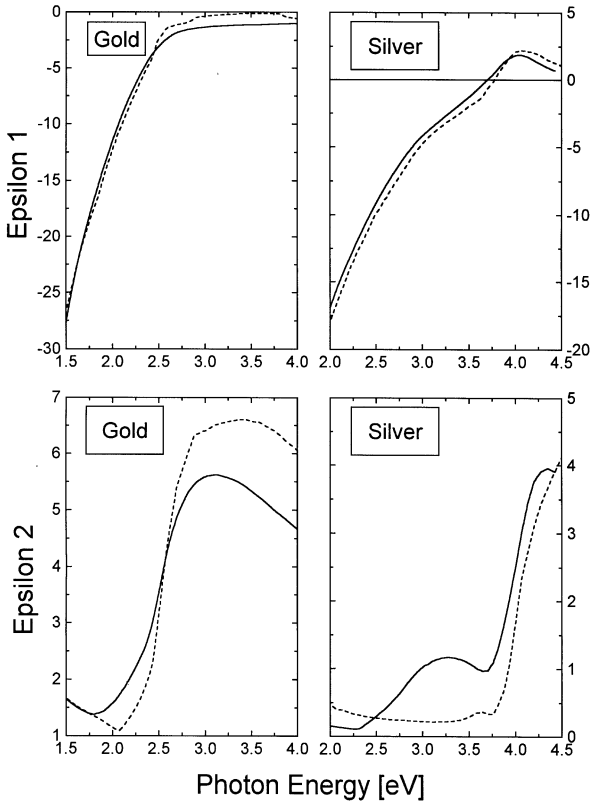

Fig. 4. "Bulk" dielectric constants of gold and silver clusters, derived from the dielectric constants of Fig. 3. For comparison, the dielectric constants of the data from Johnson and Christy [15] are plotted as dashed line

and Christy. The main differences are in the imaginary parts. The band edges of gold at 2.5 eV and of silver at 4.0 eV are similar to those obtained from evaluation of the data of Johnson and Christy [15]. However, the interband transitions begin to contribute to the dielectric constant already at lower photon energies, yielding an increased imaginary part ε_2 at photon energies of the corresponding cluster plasmon. For silver there is a small peak in ε_2 between 3 eV and 3.3 eV. This feature is also apparent in the data of Johnson and Christy but at 3.65 eV photon energy and its magnitude is quite small. The origin of this feature is still unknown. At photon energies lower than 1.8 eV for gold and 2.4 eV for silver, the imaginary part again increases with decreasing photon energy. This increase is caused by the Drude dielectric constant which only contributes to ε_2 in this region. Therefore, it was possible to fit the data on pure Drude dielectric constants, resulting in $\chi_{\text{interband},1}(0) = 7.2 \pm 0.1$ for gold and $\chi_{\text{interband},1}(0) = 2.25 \pm 0.1$ for silver.

The advantage of these unique sets of optical constants is that the position of the cluster plasmon is now fitted very well for each particle size, in contrast to the data of Johnson and Christy [15]. For fitting the halfwidth of the cluster plasmons only a size-dependence of the Drude dielectric constant according to the model of the mean free path effect must be considered. It has been proved by extensive computations according to Mie's theory [1], that in connection with the given unique dielectric constants good agreement with the experimental extinction spectra of the samples Au1, … ,Au5 and Ag1 … ,Ag5 can be obtained using one mean free path parameter $A = 0.7$ for all gold samples and one parameter $A = 2$ for all silver samples. This result is in agreement with the various theories in references [3–11], where the parameter A is material-dependent but not size-dependent. The increased A for silver must be the result of additional damping due to adsorbates, according to the theory of Persson [29].

6. Conclusion

In this paper, a method is presented which allows the determination of the dielectric constant of clusters from measured extinction spectra. It is based on a Kramers-Kronig relation for the extinction, which can be easily measured on ensembles of isolated clusters, and a generalized Newton-Raphson iteration method.

Applying this method to extinction spectra of gold and silver clusters of various sizes, the dielectric constant of the clusters was obtained at photon energies between 1.5 eV and 4.5 eV. This region includes also the interband transitions in silver clusters. The obtained data showed a clear dependence on the size and changes in the interband transition region with respect to data from literature (Johnson and Christy [15]). With the model of the mean free path effect for clusters [3–11], the data could be qualitatively interpreted. However, for silver the obtained mean free path parameters A were strongly increased with respect to those obtained in various calculations [3–11]. A first step to understand the origin of the increase in A was given by Persson [29] who considered in detail the influence of a surface layer of adsorbed molecules on the damping rate of the surface plasmon. Compared to previous papers of Kreibig [12, 13] which were also concerned with the determination of the dielectric constant of gold and silver particles, the present data extend these previous results to much larger particles and to a larger spectral range.

In addition, "bulk" optical constants for each gold and silver clusters could be derived with the help of the model of the mean free path. They can be universally used for simulation of the optical extinction by gold and silver clusters of arbitrary size. For a correct treatment of the halfwidth of the surface plasmon solely a proper mean free path parameter A must be chosen. It has been proved for all evaluated samples that only one parameter $A = 0.7$ for gold and $A = 2$ for silver has to be chosen for good agreement with measured extinction spectra when using the unique data sets for gold and silver. However, it must be emphasized that these parameters hold only for aqueous colloidal gold and silver suspensions. For other matrices they may change but should stay independent of particle size.

References

1. Mie, G.: Ann. Phys. **25**, 377 (1908)
2. Gans, R.: Ann. Phys. **37**, 881 (1912)
3. Kawabata, A.: J. Phys. Soc. Jpn. **29**, 902 (1970)

4. Kubo, R.: Polarisation, matière et rayonnement, Paris: Presse Université de France 1969
5. Kawabata, A., Kubo, R.: J. Phys. Soc. Jpn. **21**, 1765 (1966)
6. Ascarelli, P., Cini, M.: Solid State Commun. **18**, 385 (1975)
7. Ruppin, R., Yatom, H.: Phys. Status Solidi (b) **74**, 647 (1976)
8. Genzel, L., Martin, T.P., Kreibig, U.: Z. Phys. B **21**, 339 (1975)
9. Genzel, L., Kreibig, U.: Z. Phys. B **27**, 37 (1980)
10. Apell, P., Monreal, R., Flores, F.: Solid State Commun. **52**, 971 (1984)
11. Monreal, R., Giraldo, J., Flores, F., Apell, P.: Solid State Commun. **54**, 661 (1985)
12. Kreibig, U.: Z. Phys. **234**, 307 (1970)
13. Kreibig, U.: J. Phys. IV, Colloque C2, 97 (1977)
14. Landau, L.D., Lifshitz, E.M.: Lehrbuch der theoretischen Physik VIII: Elektrodynamik der Kontinua, Chap. IX, Sect. 62, pp. 302. Berlin: Akademie Verlag 1977
15. Johnson, P.B., Christy, R.W.: Phys. Rev. B **6**, 4370 (1972)
16. Hagemann, H.J., Gudat, W., Kurz, C.: J. Opt. Soc. Am. **65**, 742 (1975)
17. Olson, C.G., Lynch, D.W.: in: Behrens, H., Ebel, G. (eds.) Physics data: optical properties of metals, part II. Karlsruhe: Fachinformationszentrum Energie, Physik, Mathematik GmbH 1981
18. Garbowski, L.: Ber. dt. chem. Ges. **36**, 1215 (1903)
19. Zsigmondy, R.: Das kolloide Gold. Leipzig.: Akademische Verlagsges ellschaft: 1925
20. Kreibig, U., Genzel, L.: Surface Sci. **156**, 678 (1985)
21. Zaremba, E., Persson, B.N.J.: Phys. Rev. B **35**, 596 (1987)
22. Kreibig, U.: Z. Phys. B**31**, 39 (1978)
23. Charlé, K.-P., Frank, F., Schulze, W.: Ber. Bunsenges. Phys. Chem. **88**, 350 (1984); Charlé, K.-P., Schulze, W., Winter, B.: Z. Phys. D **12**, 471 (1989)
24. Kreibig, U.: J. Phys. F **4**, 999 (1974)
25. Hövel, H., Fritz, S., Hilger, A., Kreibig, U., Vollmer, M.: Phys. Rev. B **48**, 18 178 (1993)
26. Hövel, H.: Doctor thesis. Aachen: RWTH 1995
27. Hilger, A.: Diploma thesis. Aachen: RWTH 1994
28. Nusch, I.: Diploma thesis. Aachen: RWTH 1994
29. Persson, B.N.J.: Surface Sci. **281**, 153 (1993)